Dear author,

In the stage of preparing your full work for evaluation, after receiving approval of the corresponding abstract, we kindly ask you to follow the next steps:

,

1. Update your approved abstract (you might want to introduce modifications) and submit it now in a written version according to the abstract template (many abstracts were introduced directly into the web system). This version of the abstract will compose the *abstracts booklet* to be distributed to the participants when registering;

2. Fill the form in the next page, indicating to which section you would like your work to be directed. This will help organizing the sessions according to the mini-symposia advertised rather than in the areas and subareas present in the web system. We apologize for this possible confusion. The reason is that we are using the web system provided by ABCM, which does not allow us to introduce thematic sessions freely.

If any doubts arise, please contact us.

Your presence in MecSol 2017 will help making this a very successful event. We look forward to seeing you in Joinville!

With kind regards,

The Organizing Committee
MecSol 2017

6th International Symposium on Solid Mechanics

Click on the box to select the Mini-Symposia:

☐ Multiaxial and Fretting Fatigue (*Edgar Mamiya* and *Lucival Malcher*);

☒ Composite Materials (*Ricardo de Medeiros*);

☐ Constitutive Models I – Plasticity and Damage (*Lucival Malcher*, *Miguel Vaz Jr.* and *Edgar Mamiya*);

☐ Constitutive Models II – Viscoelastic and Viscoplastic Solids: Models and Applications (*Heraldo Mattos*);

☐ Impact Engineering (*Marcílio Alves*);

☐ Structural Reliability Methods and Reliability-Based Design Optimization (*André Beck*);

☐ Topology Optimization of Multifunctional Materials, Fluids and Structures (*Eduardo Lenz Cardoso* e *Emilio Carlos Nelli Silva*);

☐ Topological Derivatives: Theory and Applications (*André Novotny*);

☐ X-FEM, G-FEM and Meshfree Methods (*Roberto Dalledone Machado* and *Rodrigo Rossi*);

☐ High Order Finite Elements (*Marco Lúcio Bittencourt*);

☐ Nonlinear Analyses (*Eduardo Campello*);

☐ Other section;

MECSOL Joinville 2017

April 26-28, 2017
Joinville, Santa Catarina, Brazil

Prediction of Shape Distortions in Angled Composite Structures

Olumide Mayowa Makinde
Aeronautical Engineering Division
Technological Institute of Aeronautics-ITA
olumidemakinde@yahoo.com

Alfredo Rocha de Faria
Aeronautical Engineering Division
Technological Institute of Aeronautics-ITA
arfaria@ita.br

Maurício Vicente Donadon
Aeronautical Engineering Division
Technological Institute of Aeronautics-ITA
donadon@ita.br

ABSTRACT

Shape distortions, which are also known as spring in, are a major source of problems for composite manufacturers. These shape distortions are usually accompanied by built up residual stresses. They can deform a component so that it becomes useless. It also has the capability to reduce the strength of the structure. In this paper, a three-dimensional version of the plane-strain constitute model originally proposed by Svanberg and Homberg is employed to predict the shape distortions of various L-shaped composite structures. The model takes into account important mechanisms such as thermal expansion, resin shrinkage and frozen-in strains developed during curing cycles. The model was implemented into ABAQUS Finite Element code as a user subroutine UMAT. The macromechanical properties of each composite layer were predicted using a micromechanics based approach, implemented into MATLAB. A very good agreement between predictions obtained using the proposed 3D model, experimental and numerical results available in the open literature was found. Additionally, a parametric study was also performed on L shaped angled composite structures with different variations in order to evaluate their effects of the residual stresses developed during the curing process on the final geometry of the component. The simple regression model developed from the study enabled the predictions of spring in while taking into account various contributions of fiber volume, initial angle and inner radius of the composite part. The model is fairly accurate and can predict comfortably the spring in of various L shaped structures.

Keywords: Residual stresses, Shape distortions, Spring-in, Composite

1 INTRODUCTION

Distortions and residual stresses are inherently present in composite structures. Distortions are undesirable effects of the fabrication processes since they deviate the structure from nominal geometry; which can in turn compromise aerodynamic performance or make difficult the assemblage of structural components. In the same vein, residual stresses are the driving mechanisms for induced

distortions. These stresses have the potential to significantly and adversely reduce the strength of composite structures [1]. In view of the above, a lot of research effort has been geared towards the understanding and the prediction of shape distortions and residual stresses due to fabrication processes.

For thermoset composites, research has shown that there are several contributory factors that dictate the level of shape distortion and residual stresses. These factors can be divided into intrinsic and extrinsic factors. Intrinsic factors include, anisotropic thermal contraction and expansion, resin shrinkage, matrix type which affect resin shrinkage, fiber type and fiber volume fraction. Extrinsic factors include cure schedule, shape and size of the structure, type of mold and tool part interaction among others [2]. All these factors have various contributions to shape distortions and residual stresses in the structure. Anisotropic thermal contraction and expansion effects have been relatively well understood, deformation occurs from difference in temperature between the highest curing temperature and room temperature. This deformation is reversible if the structure is reheated. For resin shrinkage in thermoset composites, crosslinking of the polymer leads to shrinkage. This shrinkage produces irreversible deformation because it occurs due to the curing chemical reaction taking place. Once a resin is fully cured, resin shrinkage cannot occur any longer. Frozen-in strains are deformations that are locked into the specimen when the specimen transforms from a rubbery phase to a glassy state during in-mold cure phase of the structure.

Manufacturing deformations are particularly pronounced in structures with corner sections. Corner sections usually come out with a smaller angle than the corresponding angle of the mold and this phenomenon is called spring-in. In this paper, a three-dimensional version of the constitutive model originally proposed by Svanberg and Homberg is employed to predict the shape distortions of various L-shaped composite structures at various initial angles, fiber volume fraction, lay-up and inner radius of the part. The model captures important mechanisms such as thermal expansion, resin shrinkage and frozen-in strains developed during curing cycles. A three dimensional approach was chosen because it gives the freedom to model structures with varying thicknesses and profile while still retaining the necessary accuracy desired. Furthermore, it also gives the freedom to capture the interaction and contributions of the individual plies to the overall result if required. The study aims at showing the contribution of various initial angles, thicknesses, fiber volume, lay-up and inner radius to the overall spring in effect.

2 BACKGROUND

In the literature, there are many models simulating shape distortions of different composite systems. Spring-in; will be used interchangeably with shape distortions in this paper; is the increase of the external angle in a corner of a composite component after curing as shown in Figure 1 below. Radford and Rennick showed in [3] that the spring-in angle, $\Delta\theta$ for corner sections can be predicted from geometry and expansion strains by using equation (1) below.

$$\Delta\theta = \theta\left[\frac{\varepsilon_1 - \varepsilon_3}{1 + \varepsilon_3}\right] \approx \theta(\varepsilon_1 - \varepsilon_3) \tag{1}$$

where ε_1 and ε_3 are the free expansion in the in-plane and through-thickness directions respectively. $\Delta\theta$ is the spring-in angle and θ is the angle surrounded by the bend. In this way, the strains due to

thermal expansion and cure shrinkage can be accounted for. Equation (1) can be modified to capture the contributions of thermal expansion and cure shrinkage as described in equation (2) below

$$\Delta\theta = (\theta - 180)\left[\frac{(\alpha_1 - \alpha_3)\Delta T}{1 + \alpha_3 \Delta T} + \frac{\beta_1 - \beta_3}{1 + \beta_3}\right] \quad (2)$$

Where ΔT is the change in temperature, α_1 and α_3 are the coefficient of thermal expansion in the in-plane and transverse directions respectively. Also, β_1 and β_3 are the coefficient of chemical shrinkage in the in-plane and transverse directions respectively. This equation can be used to predict spring-in of angled shaped components, it does not capture the effect of other contributors such as frozen in strains to the spring in phenomenon.

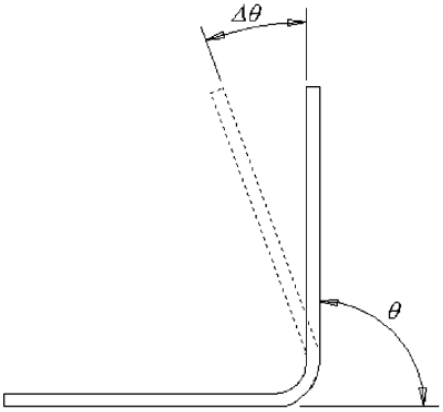

Figure 1: Angle section showing spring-in [4]

Huang et al in [5] investigated experimentally the spring in in advanced composite tools (ACT) with varying angles and radii. It was concluded that the spring-in angle decreases as the mold angle increases, but it is independent of the mold radius. Wiersma et al in [6] investigated the contributions of various factors to the spring in effect. It was concluded that the spring in cannot be predicted completely from the mismatch in thermal shrinkage due to cooling from the stress free temperature to the ambient temperature; the prediction is about 67% of the actual value for all lay-ups.

Dong et al in [7] used a FEA-based dimension variation model to predict deformations of typical composite structures. Thereafter, a regression-based dimension variation model were developed to provide a quick reference guide for prediction of several shapes. However, the regression model shown in equation (3) did not consider the contribution of the initial radius of the structure; which according to Huang [5]; contributes significantly to the spring-in effect. The model did not capture some other structural shapes like Z shape and top hat shaped structure. Dong in Ref [8] investigated the use of effective coefficients of thermal expansion in 3D modelling for spring in prediction. He observed that layer-wise modelling for spring in can be laborious and computationally expensive. Using the effective CTE (Coefficient of Thermal Expansion) in 3-D finite element analysis, the results showed good agreement with the layer-wise approach. This approach reduced significantly the number of elements and the computation time.

$$\Delta\theta = C_1(-0.826 + 0.951V_f)\frac{(180-\theta)}{90} \tag{3}$$

Fernlund et al in [9] used a 6-step method that uses a two-dimensional (2D) special purpose finite element (FE) based process simulation code and a standard 3D structural FE code. The approach avoids the need to develop a full 3D process model, significantly reducing the computational effort yet retaining much of the detail required for accurate analysis.

Svanberg in [4] presented experimental data for spring-in of glass fiber epoxy composites. The experiments were performed with angle brackets manufactured by RTM, in a steel mold with accurate temperature control. Different in-mold temperature were used to point out and separate different mechanisms responsible for spring-in. The investigation revealed that three mechanisms were majorly responsible for the spring-in phenomenon observed. The investigation also revealed that the cure schedule affects spring-in. The three mechanisms responsible for the shape distortions are: thermal expansion (different in glassy and rubbery state), chemical shrinkage and frozen-in deformations. A simple spring-in model that accounts for these mechanisms was used to illustrate and separate the contribution from each mechanism at different cure schedules, showing that they are all significant. The work concludes that constitutive models for the curing matrix and models for residual stress development and shape distortions must be able to treat both thermal effects, including glass-rubber transitions, and chemical shrinkage as well as frozen-in deformations caused by constraints experienced by the structure while undergoing in-mold cure.

Svanberg and Holmberg in [10] presented a simple mechanical constitutive model that accounted for thermal expansion, chemical shrinkage and finally frozen-in deformations. The model is a limiting case of linear visco-elasticity that removes the need for rate dependence and replaces it with path dependence on the state variables: strain, degree of cure and temperature. The model, which was derived in incremental form, is applicable for a homogenized curing composite. The accuracy of the model showed that it could be used to study various angled structures and could be used to predict trends more accurately than the Radford and Rennick equation. Svanberg and Holmberg constructed a constitutive model including different glassy and rubbery material properties and chemical shrinkage. Svanberg et al in [11] validate the simplified material model developed in the companion paper in [10] for a material and cure schedule typical for RTM and autoclave processes. Comparisons between predicted and experimental shape distortion showed that the model and simulation approach used captured both effects from different cure schedules as well as the mechanical interaction between composite and tooling during in-mold cure. The results show that changing the mechanical boundary conditions significantly affects the shape distortion prediction. Therefore accurate modelling of the composite tooling interaction is an important part of a shape distortion analysis.

In this study, various structural sections are examined in ABAQUS using a three-dimensional version of the plane-strain constitutive model originally proposed by Svanberg and Homberg in [10]. The model is employed to predict the shape distortions of various L-shaped composite structures. The model was implemented into ABAQUS Finite Element code as a user subroutine UMAT. The macro-mechanical properties of each composite layer were predicted using a micromechanics based approach, implemented into MATLAB. Additionally, a parametric study; using regression-based dimension variation model; was performed on angled composite structures with different geometries. This was done to provide a quick reference guide for prediction of several shapes. The factors considered include thickness of the structure, initial angle of the structure, lay up considerations, fiber volume fraction and radius of structure.

3 COMPUTATIONAL STUDY/EXPERIMENTAL STUDY

For the cure simulation to capture residual stress development and shape distortion, using the process model and simulation tool described in Ref [10] a number of material properties are needed. The determination of those properties is discussed below. In this study, x direction is taken along the length of the part.

3.1 Material Properties and Cure Kinetics

3.1.1 Material Properties

The materials used for the simulation was the same used by Svanberg in [4] [10] [11]. The matrix used was Araldite LY5052/Hardener HY5052 because of its suitability for Resin Transfer Molding while the Fiber used for the simulation was Hexcel 7781-127. The properties for the Araldite LY5052/Hardener HY5052 were obtained from [11] [12] and are shown in Table 1 while the properties of Hexcel 7781-127 were obtained from [11] [13] are shown in Table 2. These properties were used to calculate the lamina and laminate properties for various laminate thicknesses and lay up configurations. The lamina and laminate properties were calculated using Halpin Tsai Model [14] and 3D laminate theory [15]. The lamina properties are shown in Table 3 while the properties of the laminate are shown in Table 4. For the lamina properties, the fiber volume of 49 percent was used for the calculation. For the laminate properties, a cross ply layup of $((0/90)_s)_{16}$ was used with a thickness of 4mm.

Table 1: Mechanical Properties of Araldite LY5052/Hardener HY5052

Property	**Symbol**	**Value**		**Unit**
		Rubbery	**Glassy**	
Young's Modulus	E_m	2.8	2.6	GPa
Poisson Ratio	ν	0.5	0.38	-
Coeff. Of Thermal Exp	α	178	71	10e-6/deg Cel
Shear Modulus	G_m	9.4	0.94	GPa
Bulk Modulus	K_m	1.4	3.6	GPa
Chemical Shrinkage	β	-2.33	-2.33	%

3.1.2 Cure Kinetics

Properties of the cure kinetics were also required for the simulation. For the cure kinetics and schedule, the manufacturer's recommendation was followed. The matrix manufacturer recommends a cure schedule of 24 hours at 23ºC deg C and 4 hours at 100ºC. However, as the simulation is path based and not rate based, the time of the cure schedule would not be considered.

Also, the degree of cure at gelation was fixed at 35 percent based on data presented by the manufacturer in [12]. For the glass transition temperature T_g, the DiBenedetto equation shown in equation (4) as given by [16] is used. Where T_{go} and $T_{g\infty}$ are the glass transition temperature of the uncured (X=0) and the fully cured (X=1) respectively. For lambda (λ), the value of 0.44 was used and X is the current degree of cure.

Table 2: Mechanical Properties of Hexcel 7781-127

Property	Symbol	Value	Unit
Youngs Modulus	E_m	76	GPa
Poisson Ratio	ν	0.22	-
Coeff. Of Thermal Exp	α	4.9	10e-6/deg Cel
Shear Modulus	G_m	31.15	GPa
Bulk Modulus	K_m	45.24	GPa
Chemical Shrinkage	β	0	%

Table 3: Mechanical Properties of Hexcel 7781/ Araldite LY5052/Hardener HY5052 (V_f = 49 %)

Description	Symbol	Value		Units
		Glassy	Rubbery	
In-plane Youngs Modulus	E_l	38.59	37.26	GPa
Transverse Youngs Modulus	E_t	7.05	0.108	GPa
In-plane Poisson Ratio	ν_l	0.293	0.361	-
Transverse Poisson Ratio	ν_t	0.521	0.98	-
In-plane Shear Modulus	G_l	2.55	2.75	GPa
Transverse Shear Modulus	G_t	2.31	2.74	GPa
In-plane Coeff. Of Thermal Exp	α_l	7.17	4.97	10e-6/deg Cel
Transverse Coeff. Of Thermal Exp	α_t	50.7	136.6	10e-6/deg Cel
In-plane Coeff. Of Chem Shrinkage	β_l	-8.02E-04	-9.00E-06	%
Transverse Coeff. Of Chem Shrinkage	β_t	-0.0162	-0.0178	%

$$\frac{T_g - T_{g_0}}{T_{g_\infty} - T_{g_0}} = \frac{\lambda X}{1 - (1 - \lambda)X} \tag{4}$$

3.2 Simulation

The simulation was performed using the above mentioned properties and modifying them as required for any structure under investigation. In the simulation, a solid and homogeneous part is created for the whole laminate as recommended by Dong in [8].

3.2.1 Simulation Theory

The model as described by Svanberg in [10] is as follows. The additive decomposition of strain is assumed such that the total strain can be written as

$$\boldsymbol{\varepsilon} = \boldsymbol{\varepsilon_e} + \boldsymbol{\varepsilon_t} + \boldsymbol{\varepsilon_c} \tag{5}$$

where ε_e is the elastic strain, ε_t is the thermal strain and ε_c is chemical shrinkage strains. ε_t and ε_c are given by

Table 4: Mechanical Properties of laminate $(0/90)_{16}$

Description	Symbol	Value		Units
		Glassy	Rubbery	
In-plane Youngs Modulus	E_{11}	22.9	18.69	GPa
In-plane Youngs Modulus	E_{22}	22.9	18.69	GPa
Out-of-plane Youngs Modulus	E_{33}	8.48	2.31	GPa
Major Poisson Ratio	ν_{12}	0.09	0.0021	-
Out-of-plane Poisson Ratio	ν_{13}	0.45	0.85	-
Out-of-plane Poisson Ratio	ν_{23}	0.45	0.85	-
In-plane Shear Modulus	G_{12}	2.55	2.75E-02	GPa
Out-of-plane Shear Modulus	G_{13}	2.43	2.74E-02	GPa
Out-of-plane Shear Modulus	G_{23}	2.43	2.74E-02	GPa
In-plane Coeff. Of Thermal Exp	α_{11}	15.15	5.49	10e-6/deg Cel
In-plane Coeff. Of Thermal Exp	α_{22}	15.15	5.49	10e-6/deg Cel
Transverse Coeff. Of Thermal Exp	α_{33}	6.65	264.8	10e-6/deg Cel
In-plane Coeff. Of Chem Shrinkage	β_{11}	-3.60E-03	-7.91E-05	%
In-plane Coeff. Of Chem Shrinkage	β_{22}	-3.60E-03	-7.91E-05	%
Transverse Coeff. Of Chem Shrinkage	β_{33}	-0.0217	-0.0351	%

$$\boldsymbol{\varepsilon_t} = (T - T_0)\boldsymbol{\alpha} \tag{6}$$
$$\boldsymbol{\varepsilon_c} = (X - X_0)\boldsymbol{\beta} \tag{7}$$

where T_0 and X_0 are reference temperature and degree of cure. The coefficients of thermal expansion (α) and chemical shrinkage (β) depend on the temperature (T) and degree of cure (X) as

$$\boldsymbol{\alpha} = \begin{cases} \boldsymbol{\alpha_l}, & X < X_{gel}, \quad T \geq T_g(X) \\ \boldsymbol{\alpha_r}, & X \geq X_{gel}, \quad T \geq T_g(X) \\ \boldsymbol{\alpha_g} & T < T_g(X) \end{cases} \tag{8}$$

$$\boldsymbol{\beta} = \begin{cases} \boldsymbol{\beta_l}, & X < X_{gel}, \quad T \geq T_g(X) \\ \boldsymbol{\beta_r}, & X \geq X_{gel}, \quad T \geq T_g(X) \\ \boldsymbol{\beta_g} & T < T_g(X) \end{cases} \tag{9}$$

where the subscripts '*l*', '*r*' and '*g*' refer respectively to liquid, rubbery and glassy states. T_g is the glass transition temperature and X_{gel} denotes degree of cure at gelation. The glass transition temperature relates T_g to X by the DiBenedetto equation stated in equation (4) above. Equation (5) can be rewritten as

$$\boldsymbol{\varepsilon_e} = \boldsymbol{\varepsilon} - \boldsymbol{\varepsilon_t} - \boldsymbol{\varepsilon_c} \tag{10}$$

Equation (10) can be interpreted, as a way of determining the elastic strains, i.e., if the total strain is subtracted from the thermal and chemical strains, the remaining part is the purely elastic strain. Since the model is incremental in nature, then the incremental stresses can be written as

$$\boldsymbol{\Delta\sigma} = \begin{cases} \boldsymbol{C_r}\Delta(\boldsymbol{\varepsilon} - \boldsymbol{\varepsilon_t} - \boldsymbol{\varepsilon_c}) - \boldsymbol{s}, & T \geq T_g(X) \\ \boldsymbol{C_g}\Delta(\boldsymbol{\varepsilon} - \boldsymbol{\varepsilon_t} - \boldsymbol{\varepsilon_c}), & T < T_g(X) \end{cases} \tag{11}$$

Where C_r is the rubbery modulus tensor and C_g is the glassy modulus tensor. In the most general situation $\Delta\sigma$ contains six stress components: $\Delta\sigma_{xx}$, $\Delta\sigma_{yy}$, $\Delta\sigma_{zz}$, $\Delta\tau_{yz}$, $\Delta\tau_{xz}$ and $\Delta\tau_{xy}$. Similar observation holds for $\Delta\varepsilon$, $\Delta\varepsilon_t$ and $\Delta\varepsilon_c$, each one also containing six strain components. The incremental thermal and chemical strain computed in equations (6) and (7) are

$$\begin{aligned} \Delta\boldsymbol{\varepsilon_t} &= \boldsymbol{\alpha}\Delta T \\ \Delta\boldsymbol{\varepsilon_c} &= \boldsymbol{\beta}\Delta X. \end{aligned} \tag{12}$$

The state variables s are

$$\boldsymbol{s}(t + \Delta t) = \begin{cases} 0, & T \geq T_g(X) \\ \boldsymbol{s(t)} + (\boldsymbol{C_g} - \boldsymbol{C_r})\,\boldsymbol{\Delta}(\boldsymbol{\varepsilon} - \boldsymbol{\varepsilon_t} - \boldsymbol{\varepsilon_c}), & T < T_g(X) \end{cases} \tag{13}$$

The state variables correspond to stresses that keep track of the loading (thermal, mechanical or chemical) history. In the rubbery state the state variables become zero, meaning that the stress history has been erased. In the glassy state, the s variable represent frozen-in stresses.

3.2.2 Simulation steps

The mechanical constitutive model has been implemented in ABAQUS as a user subroutine, UMAT [17] by using an 8-node linear brick, reduced integration, hourglass control element (C3D8R). Using this subroutine, the simulation was done is 4 steps. The angle bracket was modelled with an element to represent one millimeter in the through thickness direction. Two different mechanical

boundary conditions have been used in the model. In the first case which is restricted to step 1, the whole part was fully constrained to simulate the in-mold cure phase of curing and to obtain a crude approximation of the constraint from the mould. In the remaining steps, a boundary condition to prevent rigid body motion was employed. This process simulated the demoulding process from the mould.

The Manufacturers recommended cure cycle (MRCC) was followed. The MRCC recommends that the part be cured at room temperature for 24 hours and then followed by post-curing for 4 hours at 100 degrees [12]. From the MRCC, it was stated that gel time occurs between 5 - 8 hours at room temperature. Using this information, it was assumed that gel time occurs at approximately 34 percent degree of cure. Furthermore, from the manufacturer's recommendation, the Tg attained after 1 day of room temperature cure was 55^0 which corresponds to 72 percent degree of cure using equation (4) above. This information was used in the simulation.

Step 1 was the in-mold cure, in this step, the maximum temperature which the part experienced was 23^0 (room temperature) as recommended by the manufacturer. The Tg attained after cure at room temperature is 55^0 [12]. Additionally in this step, the part undergoes 3 changes. Starting out as a liquid, with no modulus, thermal or chemical shrinkage components. Upon gelation; of which 34% degree of cure was used; it converts to rubbery state. In the rubbery state, the residual stresses gradually build up. However, as the part is fully constrained, no displacement is observed. Afterwards, the part converts into glassy state when the Tg of the part exceeds the cure temperature of 23 degrees. This occurs at around 56 percent degree of cure.

In Step 2, the part was demolded. In Step 3, the part was reheated up to 100 degrees and the matrix cure was completed before the part was cooled. It simulated a free standing position for a part that was demolded and then post cured. In Step 4, the part was finally released and the final spring–in was calculated based on nodal displacements. All the individual processes employed in the simulation are shown in Figure 2a below while all the ABAQUS steps are shown in Figure 2b below. The boundary conditions at each step was also clearly highlighted in the flowchart. Figure 3 shows the boundary conditions and the regions to which they were applied during the simulation. The combination of Figure 3(a) and Figure 3(b) alongside the symmetry boundary condition in Figure 3c accounts for the Rigid body motion constraints. Figure 3(c) shows the fully constrained boundary condition. Figure 4(a) shows the mesh used for the analysis. The density of the mesh was to ensure that the each element represents a layer of the woven fiber been simulated.

3.2.3 Simulation Results

Figure 4(b) shows the part before the simulation and after the simulation. The angular deformation was measured all through the simulation. Figure 5 below shows the deformation of the part throughout the simulation steps. Point A corresponds to the in mold cure step (Step 1). During the step, no displacement was witnessed due the in mold total boundary condition. However, residual stress build up was observed. At Point B, the fully constrained boundary condition gives way to only rigid body motion constraint. The residual stress in the part is then converted into strains. This results in the spring-in been observed at point B. Point C–D-E corresponds with the post cure process of the part. At this point, the temperature is higher than the Tg. Hence, the part is transformed from a glassy state into a rubbery state. In the rubbery state, the modulus is quite low. Therefore higher strains are witnessed in the part. Point E corresponds to the completing of the curing process. This is indicated

by the change in spring-in not resulting from the temperature application. This process occurs in step 3. At the end of the step, the part returns to room temperature at point F. The difference between point B and Point F is the frozen-in strains which occurred in the part. The spring-in given by point F is used for the parametric studies. Figure 6 shows the stress and displacement plots of the part before and after manufacture.

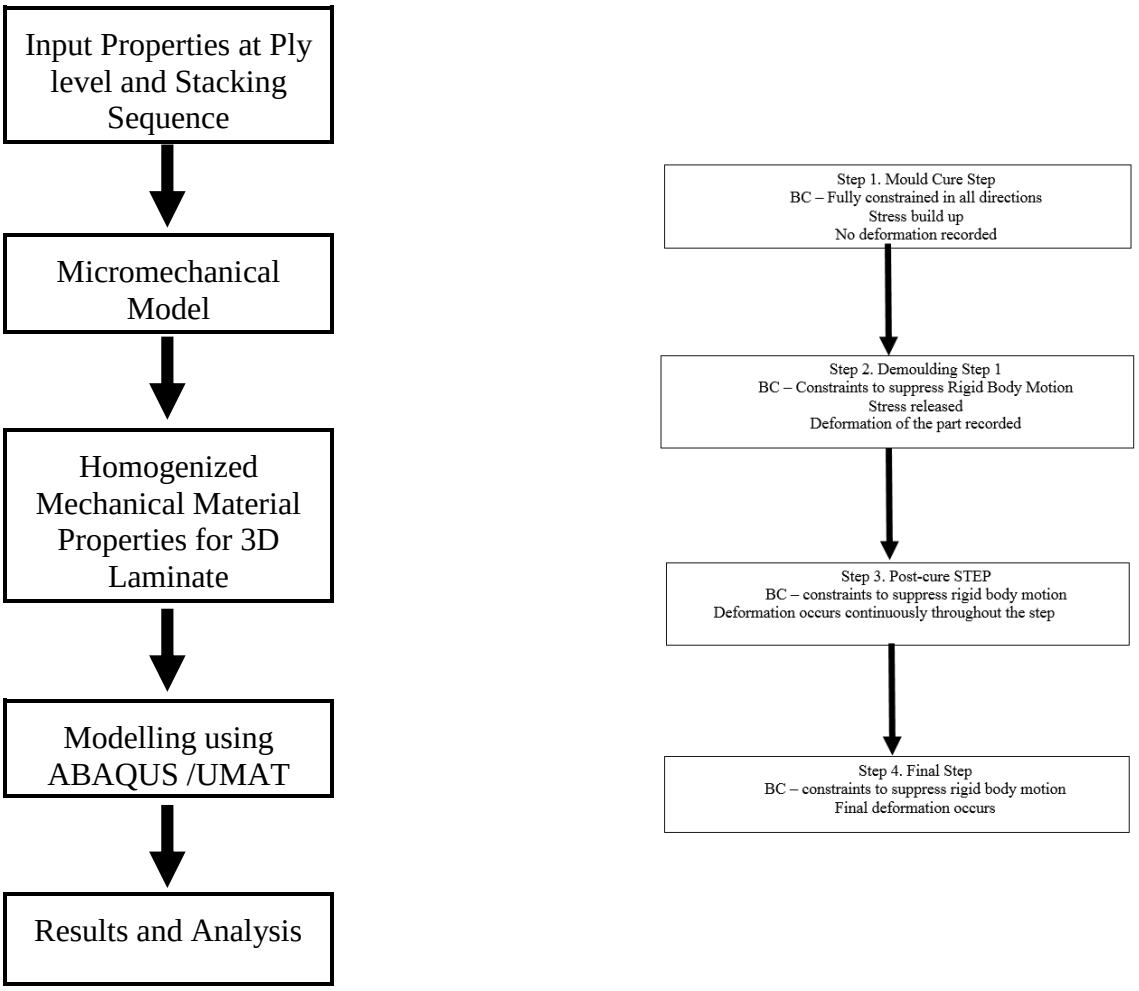

Figure 2: Simulation Flowcharts (a) shows the individual processes followed from the material up to Results and Analysis. (b) Shows the steps followed within the ABAQUS environment.

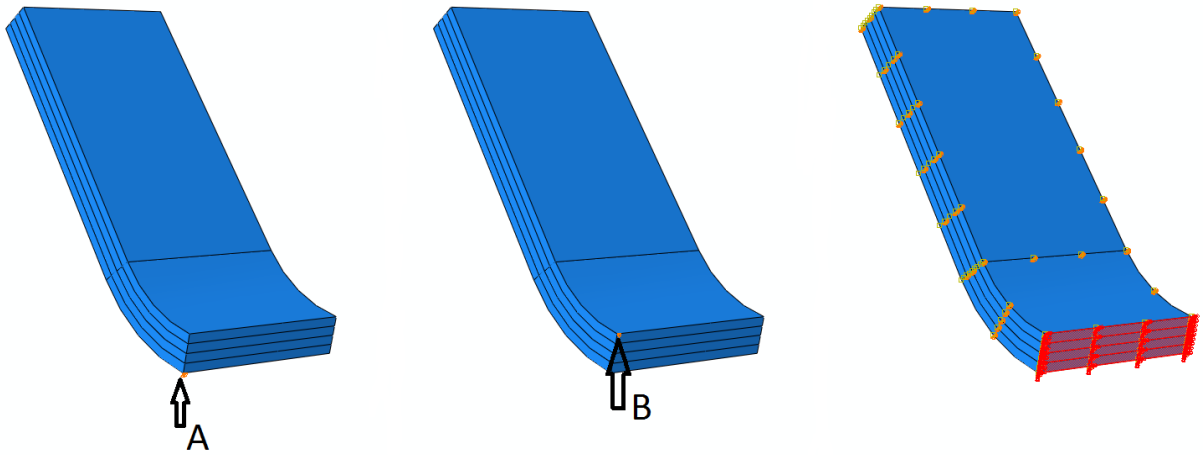

(a) (b) (c)

Figure 3: Boundary conditions for the part. (a) Shows point constrained in U1 and U3 directions (b) shows point constrained in U1 direction. (c) Shows the fully constrained boundary condition and the symmetry boundary condition. The reference coordinate of Figure 4 below is used

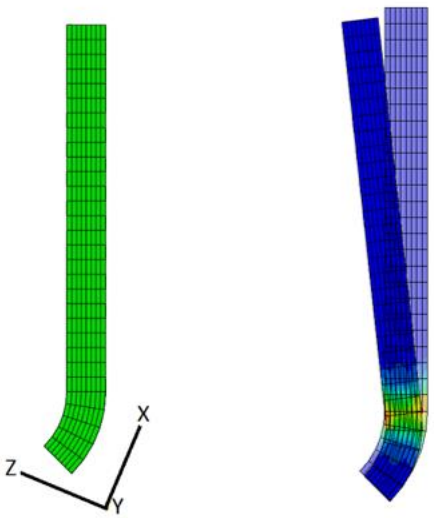

Figure 4: (a) Side view of Mesh and the reference coordinate system employed (b) The part before and after deformation

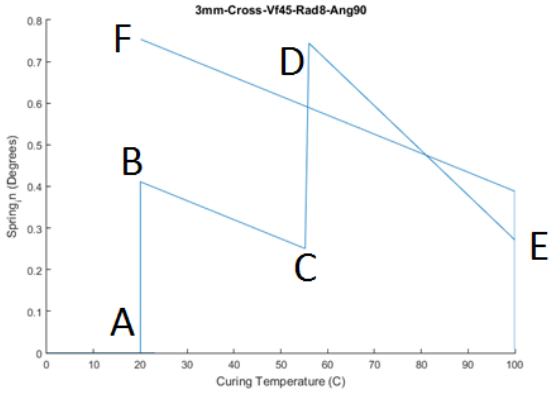

Figure 5: Angular displacement of Part during Curing Process

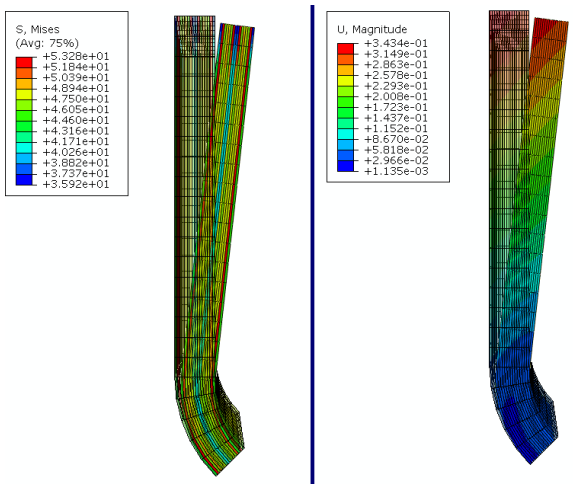

(a) (b)

Figure 6: Stress and Displacement fringe Plots. (a) shows the residual stresses present in the part after cure (b) show the deformation of the part away from the intended shape.

4 RESULTS AND DISCUSSION

The simulation was carried out on several structures. The parameters investigated are listed in the Table 5 below. The results of the various simulations are presented below.

4.1 Results

In order to the see the contribution of each of the properties to spring in, all the other properties are kept fixed while the one property is varied. This result is plotted to show the trends produced by the variation of the property. The following subsections shows the effects of different property variation.

Table 5: Parameters investigated in the Study

Initial Angle	Part Inner radius	Layups	Part thickness	Vf of Part
60	8mm	$[45/-45]_{sn}$	3mm	45%
90	10mm	$[0/90]_{sn}$	5mm	50%
120	12mm	0_n	8mm	55%

4.1.1 Effect of inner radius

The influence of the inner radius on the structure was seen to be fairly linear and constant. It shows that the inner radius has very little influence on the spring-in effect. This effect is in agreement with the Huang in [5]. Equation (14) is the trend line equations for Figure 7.

$$\begin{aligned} \Delta\theta &= 1.628 - 0.02r \quad (for\ Vf\ is\ 45\ percent) \\ \Delta\theta &= 1.386 - 0.01r \quad (for\ Vf\ is\ 50\ percent) \\ \Delta\theta &= 1.303 - 0.01r \quad (for\ Vf\ is\ 55\ percent) \end{aligned} \tag{14}$$

Equation (14) shows that the constant term has a polynomial distribution while the slopes are fairly equal to each other. Combining the equations to form one equation that captures the contribution of the three equations gives

$$\Delta\theta = 10.961 - 0.3505V_f + 0.0032V_f^2 - 0.0633r + 1e^{-3}V_f r \tag{15}$$

4.1.2 Effect of initial angle

The effect of initial angle was also investigated. The results as shown in Figure 8 below shows a downward trend as the initial angle increases. This showed that as the part tends towards been a flat plate, the spring-in influence tends to go away. This trend is in agreement with the experimental results presented by Huang et al in [5]. The trend line from the figure is shown as equation (16)

$$\begin{aligned} \Delta\theta &= 2.3 - 0.0119\theta \quad (for\ cross\ ply) \\ \Delta\theta &= 2.84 - 0.015\theta \quad (for\ angle\ ply) \end{aligned} \tag{16}$$

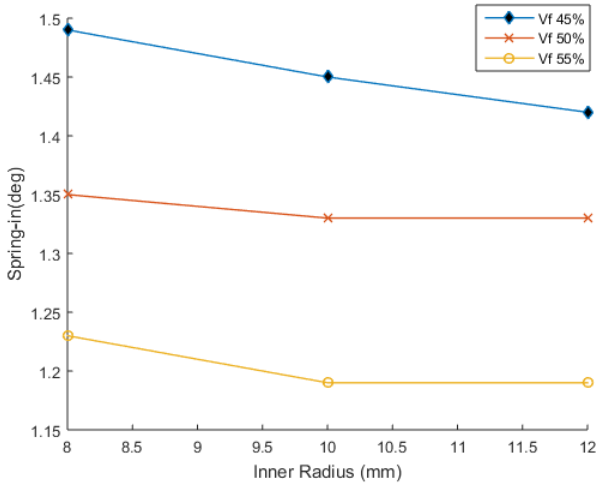

Figure 7: Effect of inner radius on spring-in

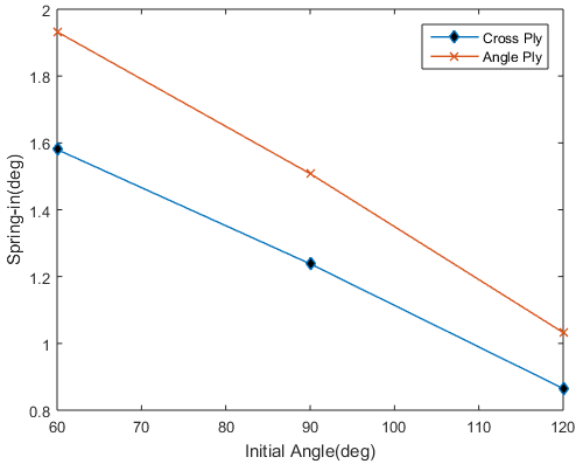

Figure 8: Effect of Initial angle on spring in

The resultant regression model for the initial angle then becomes

$$\Delta\theta = 2.57 - 0.013\theta \tag{17}$$

4.1.3 Effect of thickness

The investigation into the influence of thickness on the spring-in effect showed that the increase in thickness does not necessarily result to increase or decrease in the spring-in effect. The results for the simulations show this effect even for different fiber volumes and lay-ups. This is contrary to the postulation by Doug in [7]. The figure below shows a difference of about 2 percent between succeeding thicknesses evaluated. This is opposed to a difference of about 20 percent as shown by Doug in [7]. This means that the model does not capture the effects of thickness. This assertion requires further investigations.

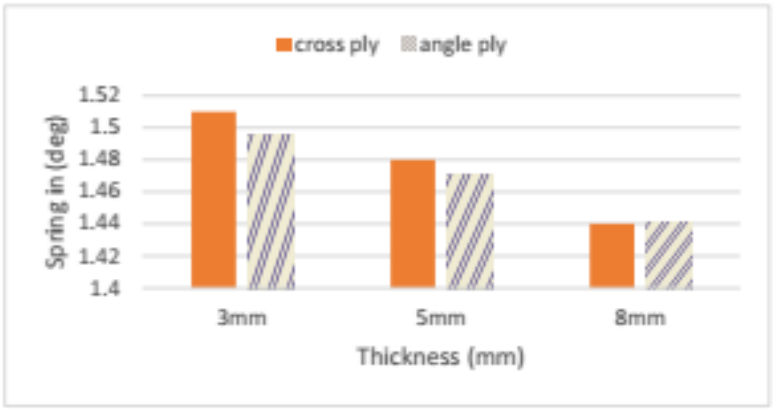

Figure 9: Effect of thickness on Spring-in

4.1.4 Effect of Fiber volume

The effect of fiber volume on spring-in was studied. The results are shown in Figure 10 below are for various inner radius and initial angle. The figure shows that there is a downward linear trend as the fiber volume increases. This is in agreement with Doug in [7]. A cursory look at the trend lines of the simulation reveals the following:

$$\begin{aligned} \Delta\theta &= 3.5052 - 0.0349V_f \quad && (\textit{for 8 mm radius at 60 deg initial angle}) \\ \Delta\theta &= 2.7348 - 0.0272V_f \quad && (\textit{for 8 mm radius at 90 deg initial angle}) \\ \Delta\theta &= 1.8724 - 0.0187V_f \quad && (\textit{for 8 mm radius at 120 deg initial angle}) \end{aligned} \tag{18}$$

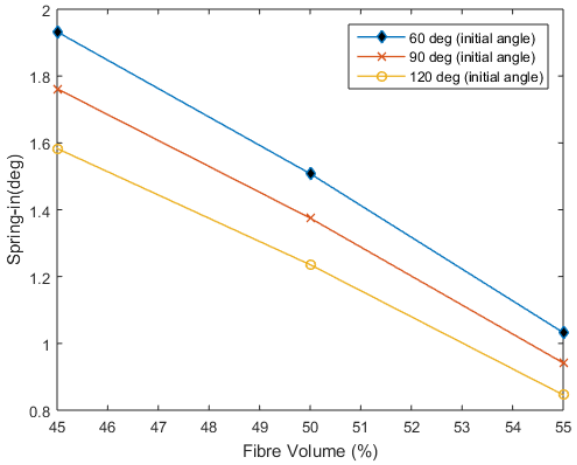

Figure 10: Effect of Fiber Volume on Spring-in

The constants of the equations have a linear distribution which can also be predicted with a trend line. Furthermore, the slopes of the equations equally have a linear disposition. Combining the trend lines for the constants and the slope gives us

$$\Delta\theta = 5.1533 - 0.0272\theta - 0.0512V_f + 3e^{-4}\theta V_f \quad (19)$$

4.1.5 Effect of Lay up

The effect of layup was investigated. The simulations was carried out on 4 parts; 0^0 unidirectional, 90^0 unidirectional, cross ply and angled plies. The results as shown in Figure 11 below showed that having layup with layers oriented in only one direction has a significant effect on the spring-in effect. The highest deformation occurred for unidirectional lay-up at 0deg while the second highest was 90^0. The cross ply and angled ply presented fairly equal results in spring in.

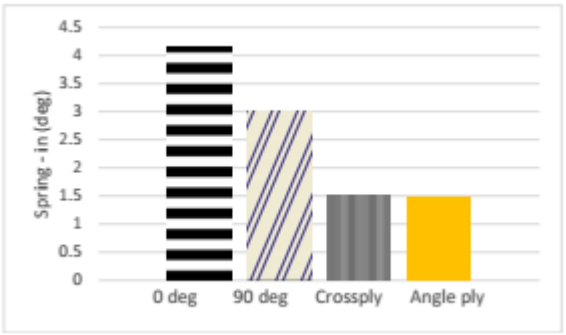

Figure 11: Effect of Layup on Spring-in

4.1.6 Overall Regression Model

Based on the models earlier described, the overall regression model can be written as equation (20). Since the contribution of the initial angle has been captured in equation (19), the effect of initial angle as described in equation (17) was no longer considered.

$$\Delta\theta = C\{8.05715 - 1.36e^{-2}\theta - 0.20085V_f - 3.165e^{-2}r + (1.6e^{-3}V_f + 0.5e^{-3}r + 1.5e^{-4}\theta)V_f\} \quad (20)$$

Where
Θ is the initial angle of the part.
R is the inner radius of the part.
C is 2.74 for 0^0 unidirectional laminate, 1.987 for a 90^0 unidirectional laminate and 1 for a cross ply laminate.
V_f is the fibre volume of the part

4.2 DISCUSSION

The model was plotted against the original ABAQUS simulation values and shown in Figure 12. It shows that the model is fairly accurate at acute initial degrees up to 90 degree with an error

percentage of less the 8 percent. However, as the initial angle of the part rises above 90 degrees, the spring in values then over-predicted by up to 30 percent of the value. Table 6 shown in the appendix is a legend showing the variables used for the simulation shown in Figure 12 below.

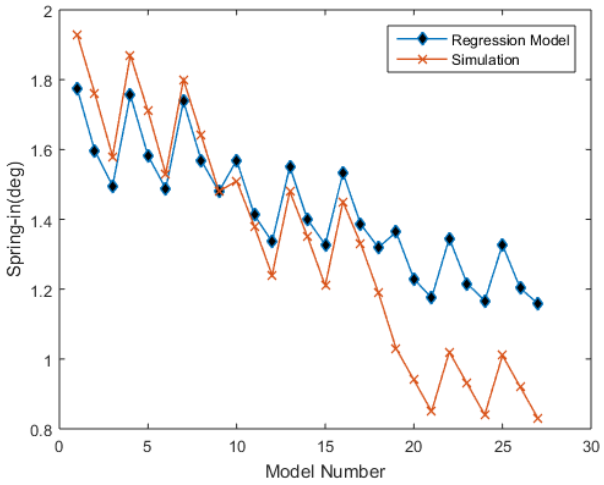

Figure 12: Comparison between fitted values and original values of Spring-in

5 CONCLUSION

In this paper, a regression-based dimension variation model was developed to accurately predict the spring in in several L shaped parts. Firstly, a three-dimensional ABAQUS model based on Svanberg's model was used to simulate several cross-sections. The model takes into account important mechanisms such as thermal expansion, resin shrinkage and frozen-in strains developed during curing cycles. The model was implemented into ABAQUS Finite Element code as a user subroutine UMAT. A very good agreement between predictions obtained using the proposed 3D model, experimental and numerical results available in the open literature was found.

The regression model was developed by first carrying out simulation on various L-shaped parts using a three-dimensional model of Svanberg's theory. The data gathered from these simulations; done by varying design parameters like Lay-up, initial angle, inner radius, fibre volume and thickness; was then used to build the model. The model also incorporates a coefficient for unidirectional, crossply and angle ply lay-up. The model was validated against the ABAQUS simulations. The results show that the model is accurate for acute angle predictions while it over predicts; by up to 25 percent; angles larger than 90 degrees. However, this can be used comfortably as a yardstick for predicting the effect various contributions to the spring-in effect.

During the simulation carried out in ABAQUS, it was discovered that Svanberg's model did not capture the effect of thickness in predicting spring-in effect. This effect requires further investigation. Furthermore, the model would be replicated for other structures like Top hat stiffeners, U shaped and Z shaped structures.

6 ACKNOWLEDGEMENTS

This work was performed in Instituto Tecnologico de Aeronatica, Brazil and was funded by the Nigerian Air Force.

REFERENCES

[1] A. R. Faria, "Prediction of post cure residual stresses and distortions in the Fabrication of Composite Structures," ITA, Sao Jose dos Campos, 2015.

[2] K. Cinar, U. E. Ozturk, N. Ersoy and M. R. Wisnom, "Modelling manufacturing deformations in corner sections made of composite materials," *Journal of Composite Materials,* vol. 48, no. 7, pp. 799 - 813, 2013.

[3] T. S. Rennick and D. W. Radford, "Determination of manufacturing distortion in laminated composite," in *Proceedings of the 11th International Conference on Composite Materials and Composite Process,* Microstruct Woodhead Publishing, 1997.

[4] J. Svanberg and J. A. Holmberg, "An experimental investigation on mechanisms for manufacturing induced shape distortions in homogeneous and balanced laminates," *Composites Part A: Applied Science and Manufacturing,* vol. 32, no. 6, pp. 827--838, 2001.

[5] C. Huang and S. Yang, "Warping in advanced composite tools with varying angles and radii," *Composites Part A: Applied Science and Manufacturing,* vol. 28, no. 9, pp. 891- 893, 1997.

[6] H. Wiersma, L. Peeters and R. Akkerman, "Prediction of springforward in continuous-fibre/polymer L-shaped parts," Department of mechanical Engineering, University of Twente, The Netherlands, 1998.

[7] C. Dong, C. Zhang, Z. Liang and B. Wang, "Dimension variation prediction for composites with finite element analysis and regression modeling,," *Journal of Composites,* vol. 35 (Part A), pp. 735 - 746, 2003.

[8] C. Dong, "Modeling the dimensional variations of composites using effective coefficients of thermal expansion," *Journal of composite materials,* vol. 43, no. 22, pp. 2639 - 2652, 2009.

[9] G. Fernlund, A. Osooly, A. Poursartip, R. Vaziri, R. Courdji, K. Nelson, P. George, L. Hendrickson and J. Griffith, "Finite element based prediction of process-induced deformation of autoclaved composite structures using 2D process analysis and 3D structural analysis," *Journal of Composite Structures,* vol. 62, pp. 223 - 234, 2003.

[10] J. M. Svanberg and J. A. Holmberg, "Prediction of shape distortions. Part I. FE-implementation of a path dependent constitutive model," *Composites part A: applied science and manufacturing,* vol. 35, no. 6, pp. 711 - 721, 2004.

[11] J. Svanberg and J. A. Holmberg, "Prediction of shape distortions. Part II. Experimental validation and analysis of boundary condition," *Composites Part A: Applied Science and Manufacturin,* vol. 35, no. 6, pp. 723 - 734, 2004.

[12] Huntsman Advanced Materials (Switzerland) GmbH, "Araldaite LY 5052/ Aradur 5052 Datasheet," Basel Switzerland , 2007.

[13] Hexcel, "HexForce Technical Fabrics Handbook," Seguin, Texas, 2010.

[14] J. C. Halpin, "Effects of Environmental Factors on Composite Materials," DTIC Document, 1969.

[15] S. W. Tsai and H.-J. Chen, "Three-dimensional effective moduli of symmetric laminates," *Journal of Composite Materials,* vol. 30, no. 6, pp. 906 - 917, 1996.

[16] L. E. Nielsen, "Cross linking effects on physical properties of Polymers," *Journal of Macromolecular Science, Part C,* vol. 3, no. 1, pp. 69-103, 1969.

[17] Abaqus, CAE, "User's manual," *Abaqus analysis user's manual,* 2011.

RESPONSIBILITY NOTICE

The authors are the only responsible for the printed material included in this paper.

APPENDIX

The table below shows the variables that were used for the simulation in Figure 12 above. The fifth column (Regression Model) gives the results for the regression model while the sixth column (ABAQUS Simulation) gives the ABAQUS results.

Table 6: Variables used for the Regression Model and Abaqus Simulations.

Model Number	Initial Angle	Initial Radius	Fibre Volume Fraction	Regression Model	ABAQUS Simulation
1	60	8	45	1.77	1.93
2	60	8	50	1.60	1.76
3	60	8	55	1.50	1.58
4	60	10	45	1.76	1.87
5	60	10	50	1.58	1.71
6	60	10	55	1.49	1.53
7	60	12	45	1.74	1.8
8	60	12	50	1.57	1.64
9	60	12	55	1.48	1.48
10	90	8	45	1.57	1.51
11	90	8	50	1.41	1.38
12	90	8	55	1.34	1.24
13	90	10	45	1.55	1.48
14	90	10	50	1.40	1.35
15	90	10	55	1.33	1.21
16	90	12	45	1.53	1.45
17	90	12	50	1.39	1.33
18	90	12	55	1.32	1.19
19	120	8	45	1.36	1.03
20	120	8	50	1.23	0.94
21	120	8	55	1.18	0.85
22	120	10	45	1.35	1.02
23	120	10	50	1.22	0.93
24	120	10	55	1.17	0.84
25	120	12	45	1.33	1.01
26	120	12	50	1.20	0.92
27	120	12	55	1.16	0.83